JGR Oceans

RESEARCH ARTICLE
10.1029/2018JC014746

This article is a companion to Kudryavtsev et al. (2019), https://doi.org/10.1029/2018JC014747.

Key Points:
- Semiempirical relations for SST and SSH anomalies derived from 20-day satellite measurements of three TCs are suggested
- SSH anomalies provide direct estimates to evaluate impact of the upwelling on amplification of the SST wake
- A marked drag reduction for wind speed higher than 35 m/s is revealed from the measured SSH anomalies

Correspondence to:
V. Kudryavtsev,
kudr@rshu.ru

Citation:
Kudryavtsev, V., Monzikova, A., Combot, C., Chapron, B., Reul, N., & Quilfen, Y. (2019). A simplified model for the baroclinic and barotropic ocean response to moving tropical cyclones: 1. Satellite observations. *Journal of Geophysical Research: Oceans*, *124*, 3446–3461. https://doi.org/10.1029/2018JC014746

Received 7 NOV 2018
Accepted 17 APR 2019
Accepted article online 29 APR 2019
Published online 31 MAY 2019

A Simplified Model for the Baroclinic and Barotropic Ocean Response to Moving Tropical Cyclones: 1. Satellite Observations

Vladimir Kudryavtsev[1,2], Anna Monzikova[1], Clément Combot[3], Bertrand Chapron[1,3], Nicolas Reul[3], and Yves Quilfen[3]

[1]Satellite Oceanography Laboratory, Russian State Hydrometeorological Unversity, Saint-Petersburg, Russia, [2]Remote Sensing Department, Marine Hydrophysical Institute, Sebastopol, Russia, [3]Laboratoire d'Oceanographie Physique et Spatiale, Institut Français de Recherche pour l'Exploitation de la Mer, Plouzané, France

Abstract Changes of sea surface temperature and height, derived from 20-day passive microwave and altimeter measurements for three tropical cyclones (TCs), Jimena, Ignacio and Kilo, during the 2015 Pacific hurricane season, sampling different stages of intensification, wind speeds, radii, Coriolis parameter, translation velocities, and ocean stratification conditions, are reported and analyzed. As triggered along the path of moving TCs, very large interior ocean displacements can occur to leave prominent sea surface height (SSH) anomalies in the TC wake. Resulting surface depressions can reach 0.3–0.5 m, depending upon size, translation speed, and ocean stratification conditions. These signatures can be quite persistent, that is, more than few weeks, to possibly be intercepted with satellite altimeters. To interpret sea surface temperature (SST) and SSH anomalies, a semiempirical framework is adopted, based on the heat and momentum conservations laws for the upper wind driven mixed layer. As interpreted, SSH anomalies provide direct estimates to evaluate the upwelling impact, that is, the upwelling amplification on the SST wake. For the reported cases, the influence of the upwelling is found rather moderate, of order 10–40%. More promising, the proposed bottom-up approach can help document the resulting wind forcing and practical drag coefficient under extreme TC conditions. As found for these three TCs, a marked drag reduction for wind speed higher than 35 m/s is inferred to ensure consistency with the measured SSH and SST anomalies.

1. Introduction

Thanks to multiple satellite remote sensing observations and improved available in situ measurements, the upper ocean responses to moving tropical cyclones (TCs) are today often very well captured and monitored (e.g., Shay, 2010, and references therein). TCs generate a variety of responses: asymmetrical sea states (e.g., Hwang & Fan, 2017; Kudryavtsev et al., 2015, Wright et al., 2001), internal motions at superinertial and inertial frequencies (Geisler, 1970; Gill, 1984; Longuet-Higgins, 1965; Meroni et al., 2017; Price, 1983), geostrophically balanced motions, and turbulence, all contributing to irreversible vertical mixing through the combination of surface stirring, shear at the base of the mixed layer, and convective cooling. As results of all these interactions and adjustments, upper ocean responses to extreme wind forcing by moving TCs still remain difficult to fully elucidate.

From a satellite perspective, distinctive features of these upper ocean transient and localized impacts attract considerable attentions. Quite systematically, TCs passages exhibit measurable persistent signatures in TC wakes, for example, changes of the sea surface temperature (SST; e.g., Cornillon et al., 1987), ocean color (e.g., Babin et al., 2004; Huang & Oey, 2015), and/or salinity (Grodsky et al., 2012; Pudov & Petrichenko, 2000). Vigorous hurricane-induced mixing and intense upwelling act to entrain cool thermocline water into the upper ocean mixed layer, stirring warm surface waters with colder waters from below. Consequently, the wake produced by the passage of a TC is generally characterized by a surface cold anomaly, accompanied with nutrient blooms and a subsurface warm anomaly (Jansen et al., 2010). As also reported, passage over freshwater plumes can cause strengthening of hurricanes due to localized enhanced SST, and minimization of the cold-water intrusion from below, due to the presence of a barrier layer effect (e.g., Balaguru et al., 2012; Reul et al., 2014).

In the Northern Hemisphere, a more or less pronounced rightward bias also occurs, consequent to TC forward motion, resulting in resonant couplings between surface winds and clockwise inertial currents,

accelerated (respectively decelerated) on the right-side (respectively left side). Mixed layer stirring and entrainment from below the thermocline are thus amplified (Huang & Oey, 2015; Price, 1981; Skyllingstad et al., 2000). Overall, TC-induced ocean cooling has then been reported to be more pronounced when the storm is intense, the mixed layer shallow with a sharp thermocline, and is slowly moving (e.g., D'Asaro et al., 2014; Lin et al., 2009; Mei et al., 2012). For the later conditions, the resulting sea state is more symmetrical, as trapped fetch effect mostly occurs for a fast-moving TC (Kudryavtsev et al., 2015). For slow-moving TCs, the circular wind pattern will further trigger Ekman pumping, driving surface water away from the storm center, with associated isopycnal uplifts that can typically reach 50–100 m (Babin et al., 2004; Walker et al., 2005).

Consequently, as mostly governed by these isopycnal displacements, TCs can also leave prominent sea surface height (SSH) anomalies in their wakes (Ginis, 2002, Figure 3). Resulting surface depressions near the storm centers, as trenches behind TCs, can reach 0.3–0.5 m, depending upon size, translation speed, and ocean stratification conditions. Following geostrophic adjustment, such a signature (encompassing barotropic and baroclinic effects) can be quite persistent, that is, more than few weeks. Accordingly, building on the actual satellite altimeter constellation (presently up to six satellites are available), satellite SSH measurements may likely cross such trenches, to provide quantitative sea surface trough amplitudes in the wakes of TCs.

In the present paper, our motivation is to essentially dwell on this overlooked capability and to report on the potential to combine SST and SSH satellite observations to analyze the ocean responses to TCs. Hereafter, this capability is demonstrated using 20-day satellite observations intercepting three major TC events, namely Jimena, Ignacio, and Kilo, developing and traveling over the central and eastern parts of the Pacific Ocean, simultaneously reaching category 4 on 29–30 August 2015 (Reul et al., 2017; Figure 7). As gathered, multisensor observations provide a comprehensive data set on local changes of SST (derived from passive microwave measurements) and SSH (altimeter measurements) along the TCs paths, sampling different stages of intensification, wind speeds, radii, Coriolis parameter, translation velocities, and ocean interior conditions. Description of the data is given in section 2. Analysis of the SST and SSH anomalies and their dependencies on TC and environment parameters, and parameterizations are discussed in section 3. In section 4, the potential to infer the hurricane-wind forcing is presented, and in section 5, the influence of the upwelling is discussed. A summary of the results is given in section 6.

2. Data

The 2015 Pacific hurricane season was the second most active one on record: 31 tropical depressions, of which 26 became named storms, and 11 major hurricanes. As already reported (Reul et al., 2017), three of these major hurricanes, namely Jimena, Ignacio, and Kilo, developed in between 20 August and 10 September. Hurricane/Typhoon Kilo became one of the longest-lived tropical cyclones on record, with a total lifespan of 22 days.

2.1. SST Wakes

Combining mult-sensor satellite measurements, daily averaged SST, at 25-km resolution (http://data.remss.com/sst/daily_v04.0/mw/2015/), are produced using optimal interpolation. For 4 September 2015, Figure 1 illustrates such a Microwave Optimally Interpolated Sea. Surface Temperatures (MW OISST) field, where black dots indicate TCs positions on this day.

While well expressed for this day, significant spatial and temporal variability of the background SST field can prevent the proper identification of these SST wakes. Commonly, differences between the SST field after and before TC passages are usually performed. The SST field averaged over 10–15 days before TC passage is then considered as the background SST field (e.g., Reul et al., 2014; Vincent, Lengaigne, Madec, et al., 2012). Yet for long time scales of order of weeks, as for the case of long-living TCs, it can be necessary to reduce as much as possible the contribution of the SST field variability. This helps focus on local features of the wake during the forced stage of its formation. Figure 2 shows fragments of the daily MW OISST data, corresponding to 3 days, 5 to 7 September 2015, around TC Kilo. For each day, its position is indicated by black dots. As revealed and anticipated, a rapid evolution of the SST wake is clearly taking place on daily time scales.

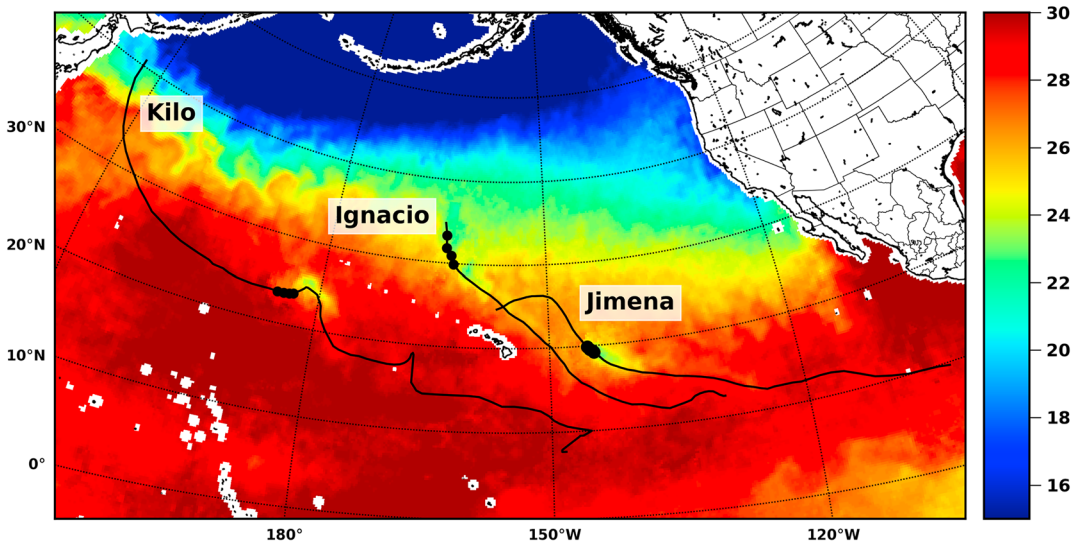

Figure 1. Daily averaged sea surface temperature field from Microwave Optimally Interpolated Sea Surface Temperature data for 4 September 2015. The black lines are the tropical cyclonesTCs' tracks according to the Best-Track Data. Black dots indicate positions of the tropical cyclone on 4 September 2015.

To best evaluate the SST anomaly, $\Delta\theta_s$, generated by a TC on a given day, t, we thus consider the difference between the SST fields, corresponding to the day after cyclone passage, $\theta_s(t{+}1)$, and 1 day before, $\theta_s(t-1)$:

$$\Delta\theta_s(t) = \theta_s(t+1) - \theta_s(t-1). \quad (1)$$

As an example, Figure 3a illustrates a field of SST anomalies (on day t corresponding to 6 September) using equation (1) and the difference between the SST fields on 7 and 5 September, shown in Figure 2. We then consider transects of the SST anomalies in the direction perpendicular to the hurricane track. Transects are then averaged along the track direction. The averaging window approximately corresponds to the distance traveled by TC during a day, Figure 3a. The averaged transect of the SST anomaly is shown in Figure 3b. The following parameters are then defined: magnitude of the SST anomaly, $\delta\theta_s$, corresponding to the minimal value of the $\Delta\theta_s(t)$ transect; right-biased offset of the anomaly, δx, defined as the distance between $\delta\theta_s$ location and TC track positions; and the anomaly width, l, defined as the distance between the isotherms equal to half $\delta\theta_s$, see Figure 3b for more explanation. Since SST anomalies are sufficiently averaged, we introduced the minimum value, $\delta\theta_s^{\min}$, as an extra characteristic of the SST wake. It is defined as the minimal value of the SST anomaly $\Delta\theta_s(t)$ found inside the averaged transect region and $\delta\theta_s^{\min} \leq \delta\theta_s$.

As illustrated Figure 4, these resulting SST wake parameters can significantly vary over the course of the TCs, corresponding to a wide range of changes in TC characteristics (i.e., maximum wind speed, translation velocity and size) and environmental conditions (i.e., ocean stratification and the Coriolis parameter). To note, the minimal value of the SST anomalies, $\delta\theta_s^{\min}$, well follows variations of the minimum of the (averaged) SST anomalies, $\delta\theta_s$, but displays some local offsets (up to about 2°).

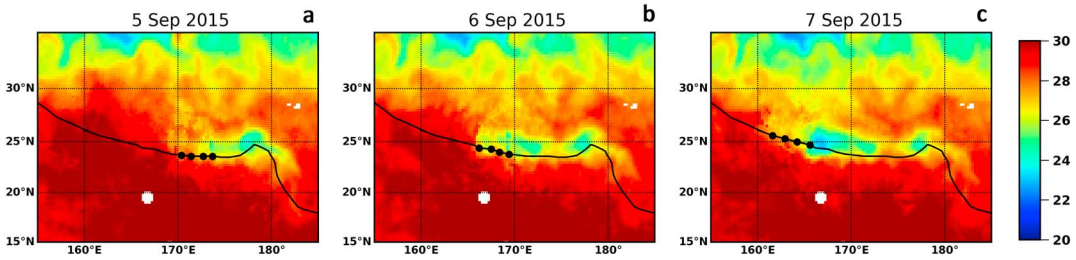

Figure 2. Daily averaged sea surface temperature fields from Microwave Optimally Interpolated Sea Surface Temperature data for (a) 5 September, (b) 6 September, and (c) 7 September 2015. Black lines is the tropical cyclone Kilo track and black dots indicate its positions within the given day.

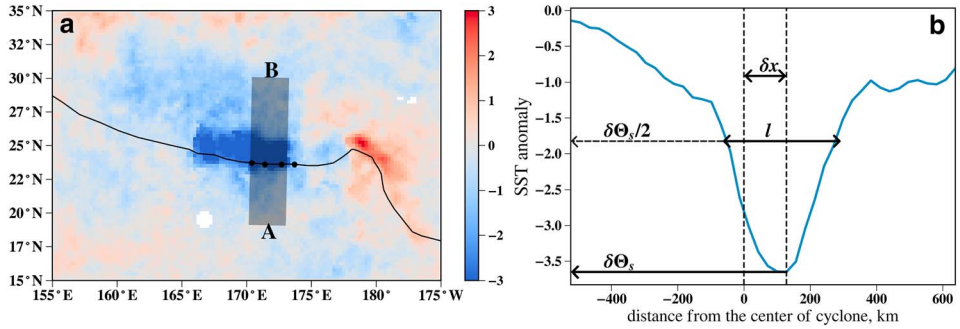

Figure 3. (a) Sea surface temperature (SST) anomaly field on 6 September and (b) profile of SST anomaly along cross section AB. The vertical dashed line crossing 0 on x axis corresponds to the position of the tropical cyclone track. Distance between two dashed lines indicates offset of the SST anomaly from tropical cyclone track; l is the width of the SST anomaly defined as distance between isotherms equal to half the SST anomaly.

2.2. SSH Wakes

The SSH anomalies are investigated using multisatellite altimeter measurements. For the study, altimeter data from three missions are used: Jason-2, CryoSat-2, and SARAL/AltiKa. The Jason-2 Geophysical Data Records (GDRs) are provided by the National Oceanographic Data Center (NODC; http://www.nodc.noaa.gov/). The CryoSat-2 data are available at the European Space Agency (ESA) Earth Online website (https://earth.esa.int/). The SARAL/AltiKa GDRs are distributed through the Archiving, Validation and Interpretation of Satellite Oceanographic data (AVISO) portal (http://www.aviso.altimetry.fr/).

Operating at high frequencies (i.e., Ku- and Ka-band), radar altimeter measurements are sensitive to precipitations, and data affected by TC rain bands can often be lost. Yet as SSH anomalies are expected to be long-living surface features, possibly persisting for several weeks, the time difference between altimeter

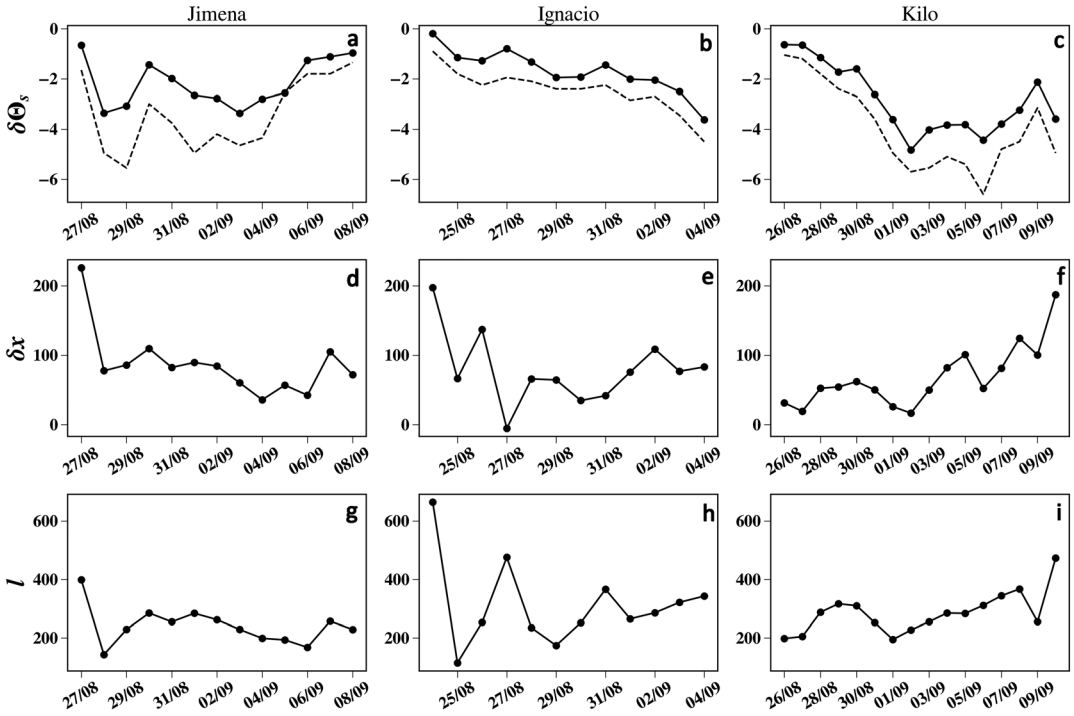

Figure 4. Time-evolution using coordinate system moving with tropical cyclone (TC) of (a–c) the sea surface temperature (SST) anomaly magnitudes (solid line corresponds to averaged SST anomaly and dashed line to the minimal value inside the averaging window), (d–f) offset of the SST anomaly from TC's track, and (g–i) width of the anomaly for TCs Jimena (a, d, and g), Ignacio (b, e, and h), and Kilo (c, f, and i).

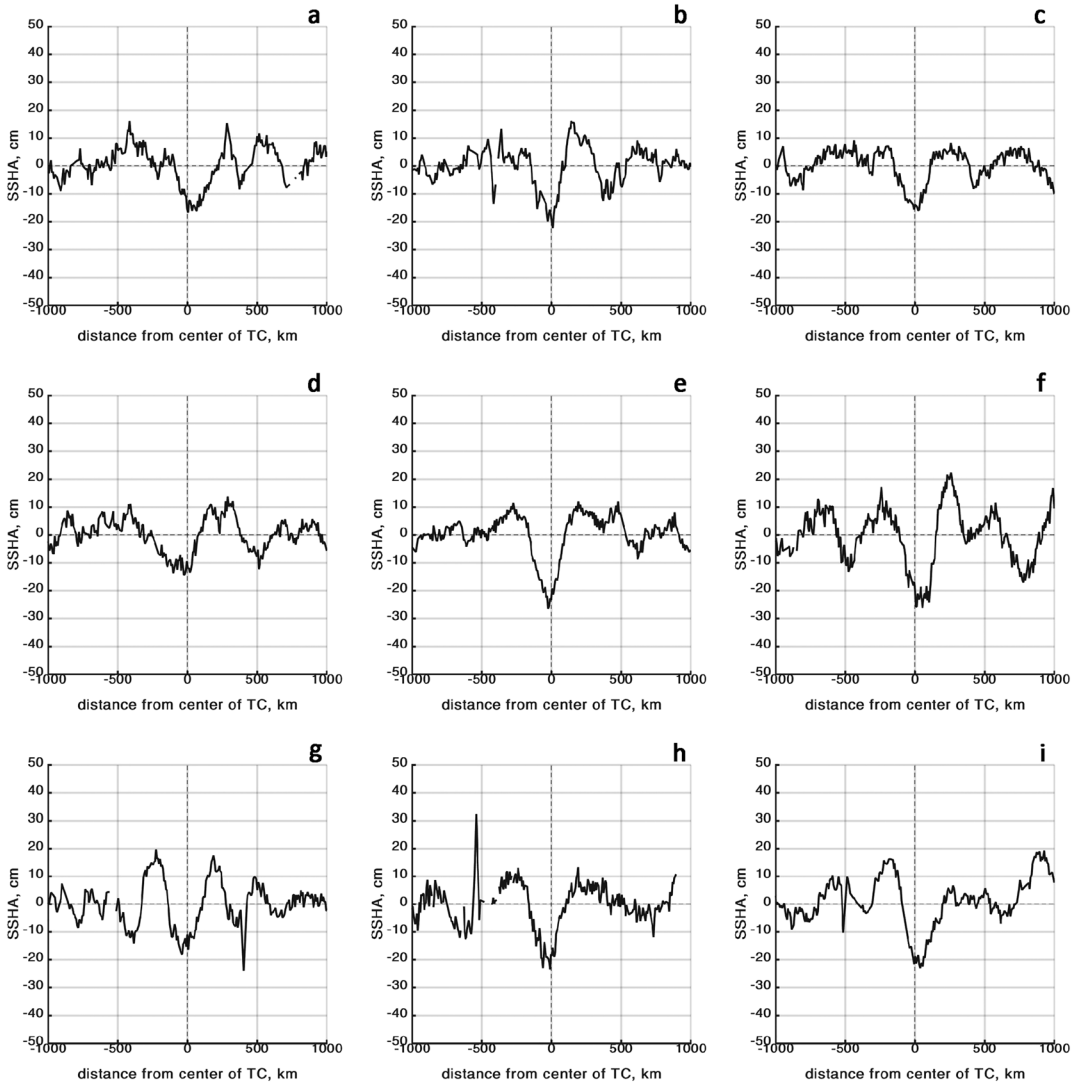

Figure 5. Examples of sea surface height (SSH) anomalies obtained from the altimeter passes crossing (a, d, and g) tropical cylone (TC) Ignacio, (b, e, and h) TC Jimena, and (c, f, and i) TC Kilo. Vertical dashed lines crossing 0 on the *x* axis indicate position of TC track taken from Best Track data. Magnitude of SSH anomaly is further defined as minimum of the surface height around TC track.

measurements, also controlled by each altimeter cycle, can be relaxed. In total, 53 altimeter passes crossing TC tracks (after a TC passage) have been selected. As selected, SSH anomalies correspond to measurements for which the time differences between altimeter crossing a TC track and the time of its passage did not exceed 6 days. Figure 5 shows examples of SSH anomalies with well expressed depressions around the TC track. Apparent oscillations apart from the TC are also revealed, to possibly be interpreted as TC baroclinic wake signatures and/or residual SSH anomalies left by other preceding TCs, previously traveling in the same area before. The maximum magnitudes of these SSH anomalies are then collected to be compared with TCs characteristics and environmental conditions.

2.3. Best Track Data

TCs trajectories and main characteristics are taken from the Best Track (BT) data (http://ftp.nhc.noaa.gov/atcf/), that is, maximum wind speed, u_m, and its radius, R_m, with translation velocity, V, derived from the TCs coordinates, Figure 6. For instance, Kilo peaked in intensity on 30 August as a category 4 hurricane with 120-kt winds. After peaking in intensity, Kilo fluctuated between categories 3 and 4, as it slowly moved northwest, before weakening below major hurricane status as conditions became less favorable. More

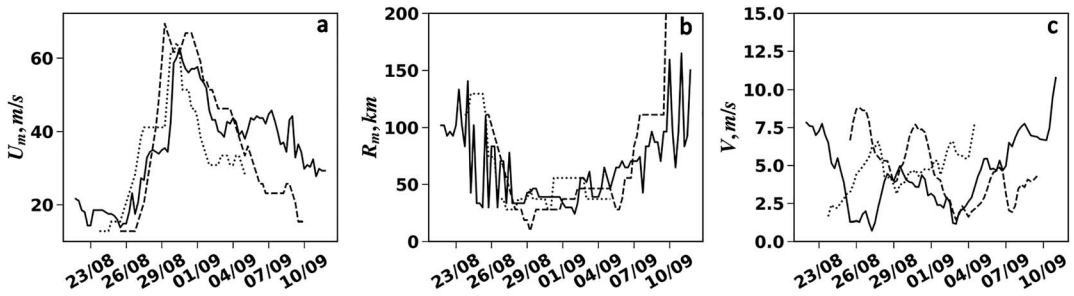

Figure 6. Along-track evolution of (a) maximum wind speed, (b) radius of maximum wind, and (c) translation velocity derived from best track data for Hurricanes Kilo (solid line), Jimena (dashed line), and Ignacio (dotted line).

detailed comparisons between BT estimates and low-frequency passive radiometer satellite measurements can be found in Reul et al. (2017).

Among key parameters to determine impacts on the upper ocean layers, the dimensionless TC translation velocity is often considered

$$Ro = \frac{V}{R_m f} \tag{2}$$

also termed as the TC Rossby number, f is the Coriolis parameter. This parameter divides TCs in two groups: "slow" if $Ro < 1$ and "fast" if $Ro > 1$. Reported observations revealed that SST anomalies generated by slow TCs are systematically larger than those generated by fast ones (Mei et al., 2012). As already mentioned above, contrarily to slow TCs, fast TCs generate right (left)-biased SST wakes in the Northern (Southern) Hemisphere (Cornillon et al., 1987).

For each TC case, evolutions of the translation velocities and Rossby numbers are given in Figure 7. As obtained, *Ro* widely varies, from almost 0 to about 10. During most of their life span, the three TCs can be classified as fast ones, and only rarely as slow TCs. Changes of TC size can impact *Ro*, and in some case, for example, for TC Jimena around 29 August, the marked decrease of the TC radius leads to *Ro* behavior opposite to the translation velocity trend. Note, these TCs were all generated in the equatorial region to then travel northward. As such, the Coriolis parameter varies by a factor 3, also contributing to strongly modulate *Ro*.

2.4. Ocean Interior

As anticipated and often reported (D'Asaro et al., 2014; Lin et al., 2009; Mei et al., 2012), resulting SST anomalies also significantly depend on the local upper ocean stratification under the moving TC. To specify a background stratification, that is, before a TC passage, ocean interior conditions are evaluated from the monthly averaged temperature and salinity data provided by the World Ocean Atlas 2013 version 2 (https://www.nodc.noaa.gov/OC5/woa13/). As a comparative ground-truth data set, ISAS-15 gridded (1/2° resolution) monthly fields and climatology of temperature and salinity is also employed, which are

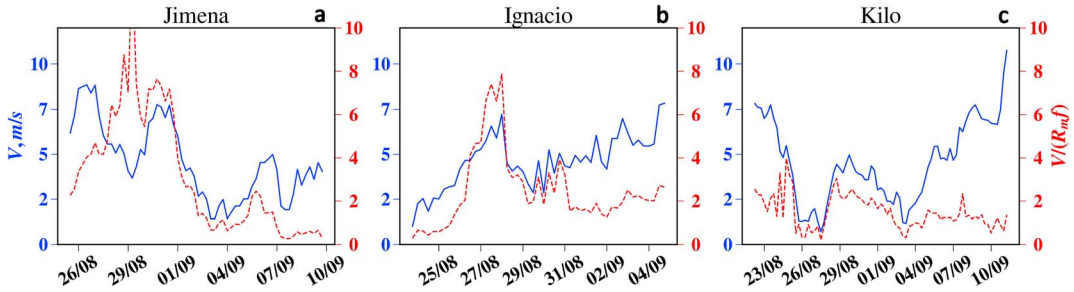

Figure 7. Along-track evolution of (red) the tropical cyclone-Rossby number, $Ro = V/(R_m f)$, and (blue) the translation velocity, V, calculated from the best track data for (a) Jimena, (b) Ignacio, and (c) Kilo.

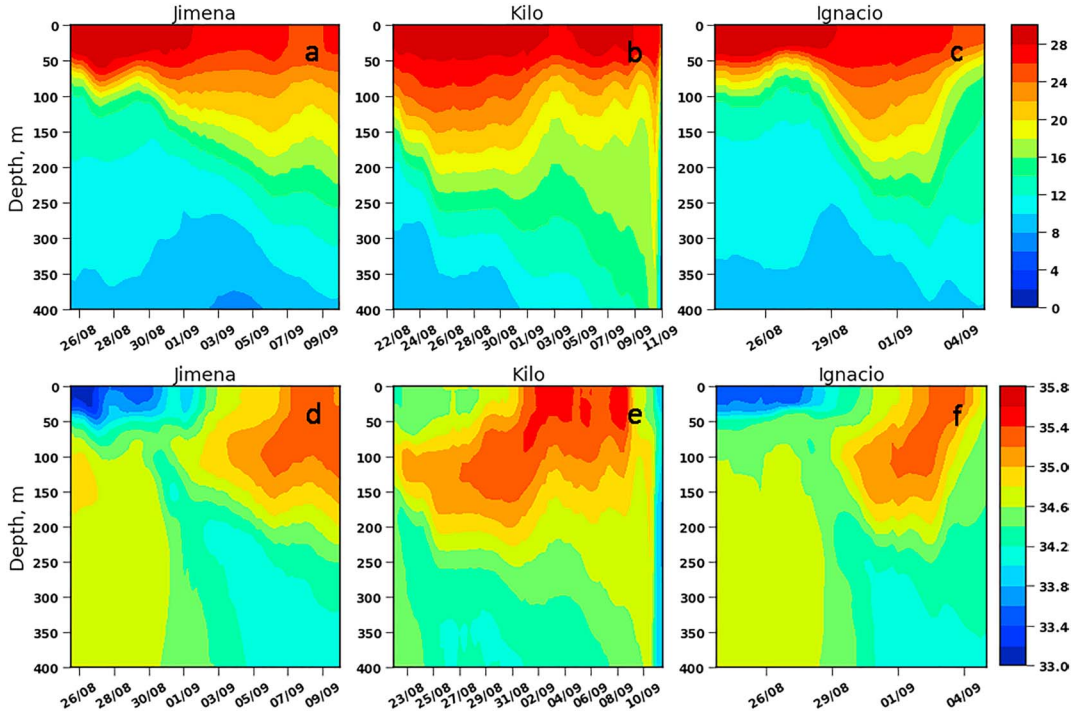

Figure 8. Vertical cross sections of the (a–c) temperature and (d–f) salinity of the upper 400 m of the ocean along the tropical cyclones tracks: (a and d) Jimena, (b and e) Kilo, and (c and f) Ignacio. The data are taken from ISAS-15 gridded (1/2° resolution) monthly fields.

constructed from ARGO profilers on 152 levels ranging from 0- to 2,000-m depth and entirely based on these in situ measurements (Kolodziejczyk et al., 2017). Resulting vertical cross sections of the ocean temperature and salinity along the TCs tracks are shown in Figure 8. As found, temperature stratification significantly varies along the TC tracks. For instance, at their initial stage of developments, Jimena and Ignacio traveled over an area with shallow thermocline, to then pursue over an ocean area exhibiting deep and smeared thermocline conditions. As also revealed, the sharp temperature drop at the end of Kilo's track, is likely related to inflow of cold freshened Arctic waters through the Bering Strait, reaching the eastern coast of Japan.

The density, ρ, is evaluated using a linear approximation for the UNESCO sea water state equation in the form

$$\rho = \rho_0[1-\alpha(\theta-\theta_0)+\beta(s-s_0)] \tag{3}$$

where $\alpha = 2.7 \times 10^{-4}$ 1/ ° C and $\beta = 7.6 \times 10^{-4}$1/‰ are thermal and salinity expansion coefficients correspondingly, θ is the water temperature in °C, s is salinity in per mille, and $\rho_0 = 1{,}025$ kg/m^3 is the reference density with $\theta_0 = 22$ ° C and $s_0 = 36$‰. From density, two stratification parameters are determined: Brunt-Väisälä frequency, N, of the upper ocean below the mixed layer, and phase velocity of long gravity internal waves contributing to the baroclinic response.

To infer these parameters, the local vertical ocean stratification (at each point of TC track) is approximated with a three-layer stratification model, adjusting the seasonal and the main pycnoclines with linear approximations of density over the depth, and the abyssal part with constant density. The fit parameters (Brunt-Väisälä frequency, N, in the seasonal pycnocline and its depth, d) are derived using a least squares method. It ensures adjustment of the model density profile in the seasonal and main pycnocline to the observed profile in the layer $h < z < D$, where h is the mixed layer bottom (identified as the maximum of the second derivative of the density profile), and D is the depth of the lower boundary of the main pycnocline, defined as the depth of the layer containing 95% of the total observed density drop. Examples of adjustments for "shallow" and "deep" pycnoclines are given in Figure 9. As a measure of the ocean stratification, Figure 10, the vertical gradient of the water temperature in the seasonal pycnocline, that is, in the layer $h < z < d$ prescribed by the three-layer model, is further estimated. It also demonstrates quite strong along-track variability.

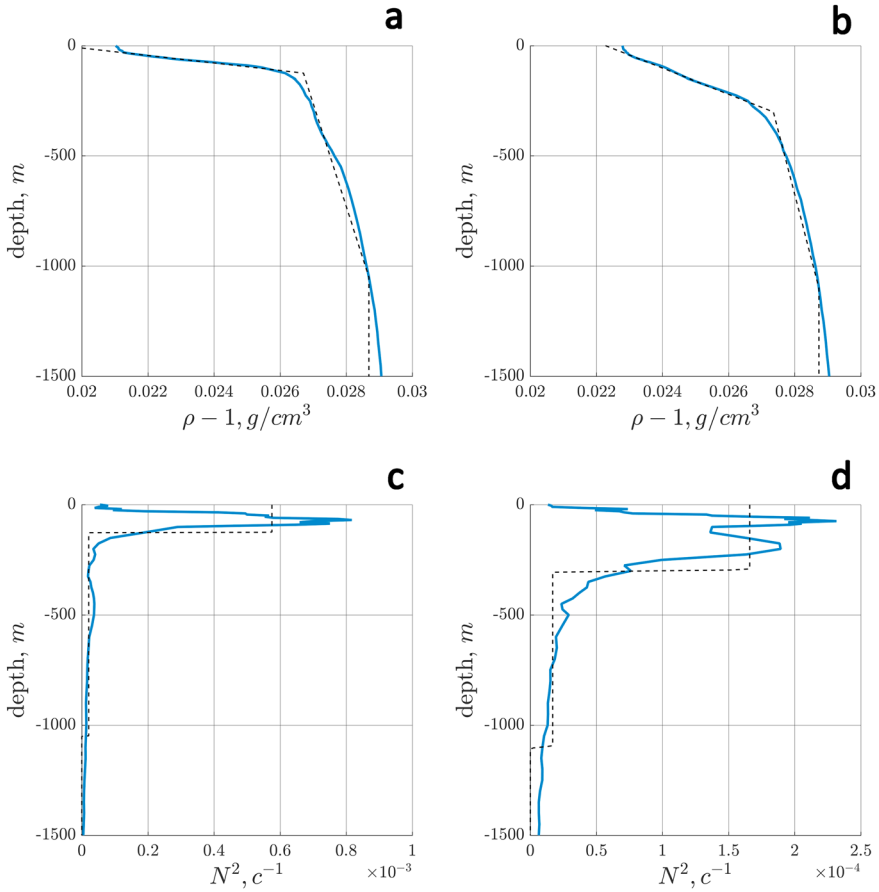

Figure 9. Solid lines are (a and b) density and (c and d) squared Brunt-Väisälä frequency profiles for the (a and c) shallow and (b and d) deep pycnoclines. Dashed lines in the upper row indicate fit of the density profiles by three-layer model, and corresponding three-layer models for N^2 are shown in plots (c) and (d).

Finally, the phase velocities, C_i, of inertial-gravity internal waves (IW) corresponding to the first three modes defined within the frame of the three-layer stratification model along the TC tracks are given, Figure 11. IW phase velocities, C_i, for each of the modes do not significantly vary. As a transient and intense extreme event, a TC will trigger baroclinic response when its translation velocity exceeds the IW phase speed, $U > C_i$. From Figure 11, it may appear that TC Ignacio, during most of its life span, is relatively fast and capable to generate baroclinic responses formed by the composition of the first three IW modes. At variance, TCs Kilo and Jimena are slower during about half of their life spans, with translation velocities below the first IW mode, and sometimes even below the second mode.

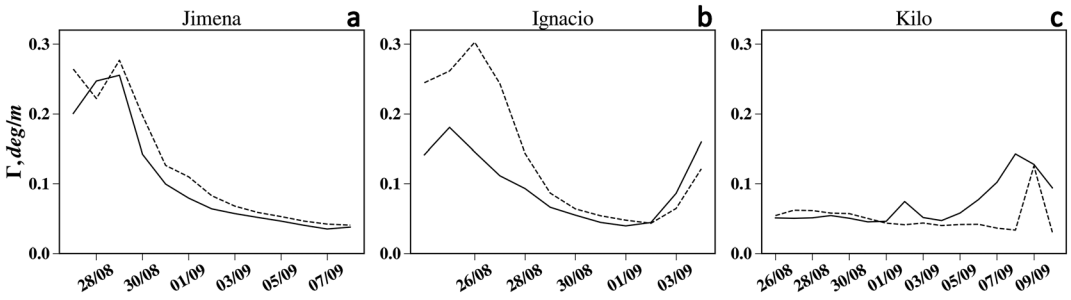

Figure 10. Along-track evolution of the local vertical gradient of the ocean temperature in the seasonal thermocline calculated from (solid lines) WORLD OCEAN ATLAS and (dashed lines) ISAS-15 gridded (1/2° resolution) monthly fields for (a) Jimena, (b) Ignacio, and (c) Kilo.

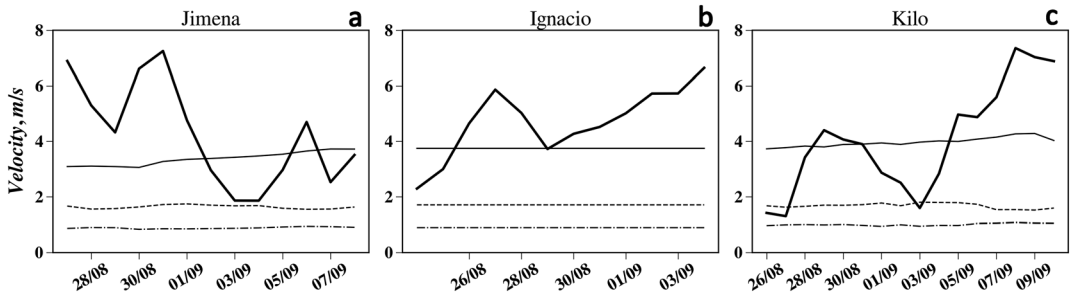

Figure 11. The along-track evolution of (thick solid lines) tropical cyclone translation velocity and internal waves phase velocity for three first modes (thin solid, dashed, and dash-dotted lines correspondingly) for tropical cyclones (a) Jimena, (b) Ignacio, and (c) Kilo.

3. Analysis and Scaling of SST and SSH Anomalies: Dependencies on TC and Environment Parameters

3.1. SST Anomalies

At first, estimated SST anomalies, $\delta\theta_s$, can be compared with concomitant maximum wind speed, translation velocity, and/or temperature gradient in the seasonal thermocline. As found (not shown), no remarkable correlation is emerging from these comparisons. An overall wind trend, that is, the higher the winds, the larger the SST anomalies, could still be revealed. This is in qualitative agreement with previously reported observations (e.g., D'Asaro et al., 2014; Lin et al., 2017). Such a weak correlation with these individual variables clearly invites to consider more elaborated combinations of parameters, to best interpret SST anomalies.

Vincent, Lengaigne, Madec, et al., 2012, Vincent, Lengaigne, Vialard, et al., 2012) introduced two variables, the Wind Power index (WPi) and the Cooling Inhibition index (CI). The WPi characterizes the strength of the TC forcing on the upper ocean and is based on the power dissipated by friction at the air-sea interface (Emanuel, 2005). It combines in a single measure, the maximum wind, TC size, and translation speed: $WPi \propto u_m(R_m/V)^{1/3}$. WPi is a proxy to estimate the available amount of kinetic energy contributing to mixing in the upper ocean and thermocline erosion, leading to surface cooling. As cooling also depends on the ocean background stratification, that is, type of the thermocline—shallow/sharp or deep/broad, CI is introduced to characterize the conversion of kinetic energy to potential energy by vertical mixing. This helps identify the possible inhibition of mixed layer deepening in presence of a strongly stratified background. From their numerical experiments, Vincent, Lengaigne, Vialard, et al. (2012) demonstrated that TC-induced SST anomalies are largely controlled by WPi and CI, with CI affecting the cooling amplitude by up to an order of magnitude.

For the present analysis, we advocate a more straightforward scaling, based on classical upper mixed layer concept. Similar to Vincent, Lengaigne, Vialard, et al. (2012), maximum wind speed, u_m, its radius, R_m, and translation velocity, V, are considered as TC governing parameters, defining the upper ocean forcing. As also expected, governing environmental parameters are, prestorm values of the Brunt-Väisälä frequency, N, temperature gradient, Γ, in the seasonal pycnocline, and Coriolis parameter, f. Considering the ocean temperature and the density to linearly vary with the depth in the seasonal pycnocline, the SST, θ_s, satisfying a 1-D heat conservation equation reads

$$\theta_s = \theta_s^0 - 1/2\Gamma(h_m + \delta h) \tag{4}$$

where θ_s^0 is the conventional "calm condition" SST of the ocean, h_m is the mixed layer depth, and δh is the displacement of the water masses at $z = h_m$ due to the TC-induced upwelling effect. In equation (4), the solar heating and other components of the heat balance are ignored, and equation (4) is thus best valid during the initial stage (forced stage) of the transient TC impact on the upper ocean. Under enhanced wind forcing, equation (4) suggests that cooling results through mixed layer deepening, caused by an intensification of turbulent mixing (this corresponds to 1-D ocean model), and through the upwelling associated to the resulting vorticity of the surface stresses. Under a three-layer approximation of the ocean stratification (see Figure 9), the vertical velocity in the upper seasonal thermocline layer, with constant N, reads:

$w(z) \propto \sin(Nz/c)$ (see, e.g., Appendix A in Kudryavtsev et al., 2019). If the TC-induced displacement of the main pycnocline, δD, is chosen as a leading parameter, then δh is evaluated as $\delta h = (h_m N_1/c)\delta D$, where we simplify, $\sin(h_m N_1/c) \approx h_m N_1/c$. Then equation (4) can be rewritten as

$$\delta\theta_s = -\frac{N^2}{2\alpha g} h_m [1 + (N_1/c)\delta D] \tag{5}$$

where $\delta\theta_s$ is the SST anomaly, and we assumed that the vertical gradient of the ocean temperature largely controls the amplitude of Brunt-Väisälä frequency, that is, $\Gamma \approx N^2/(\alpha g)$.

Following the concept of a critical regime for the mixed layer deepening (e.g., Price et al., 1986), the mixed layer may be postulated to evolve as to maintain the bulk Richardson number at a constant (critical) value:

$$Ri_{\mathrm{cr}} = (\Delta\rho/\rho) g h_m / v_m^2 \tag{6}$$

where $\Delta\rho/\rho$ is the relative density drop over the mixed layer base, and v_m is the magnitude of the wind drift current velocity in the mixed layer. The parameterization of h_m by equation (6) explains the possible offset of the SST anomalies from the TC track, since inertial drift currents are amplified to the right from the track where wind stress rotation coincides with the rotation of inertial currents (Price et al., 1986). Introducing the volume transport by the wind-driven current as $M_w = v_m h_m$, and estimating M_w from the momentum conservation as $M_w = (\tau/f)\varphi(fR_m/V)$, we further use $\Delta\rho/\rho = (1/2)h_m N^2/g$, to suggest

$$h_m = u_*/(fN)^{1/2} \varphi^{1/2}(fR_m/V) \tag{7}$$

where we took $(2Ri_{\mathrm{cr}})^{1/4} \approx 1$. For $fR_m/V > > 1$, the dimensionless function $\varphi(fR_m/V)$ shall become constant, and equation (7) reduces to a classical relation for the mixed layer depth. For $fR_m/V < < 1$, corresponding to a fast TC, function $\varphi(fR_m/V)$ shall tend to $\varphi \approx fR_m/V$. Then TC induced SST anomalies from equation (4) with equation (6) shall follow

$$\delta\theta_s \approx \left[u_* N^{3/2}/\left(g\alpha f^{1/2}\right)\right] \varphi^{1/2}(fR_m/V)[1 + (N_1/c)\delta D] \tag{8}$$

The term $[1+(N_1/c)\delta D]$ in equation (8) can be interpreted as an amplification factor of the SST anomalies due to the upwelling mechanism. Yablonsky and Ginis (2009) already pointed out that upwelling can play a significant role in the formation of SST anomalies: for a slow TC, with translation velocity less than 5 m/s, it becomes crucial. For very slow translation velocity, that is, 1–2 m/s, SST anomalies are dominated by the upwelling mechanism, and a classical 1-D ocean turbulence mixing model would not solely explain observations. As a first guess, we can thus assume the function $\varphi^{1/2}(Ro)[1+(N_1/c)\delta D]$ to mainly depend on the translation velocity, or on the TC Rossby number $Ro = V/fR_m$ in our notation. Introducing $\varphi_\theta(Ro) \equiv \varphi^{1/2}(Ro)[1+(N_1/c)\delta D]$ and scaling u_* as $u_* \propto u_m$, TC-induced SST anomalies in equation (8) shall thus well be parameterized as

$$\delta\theta_s/\langle\delta\theta_s\rangle \propto \varphi_\theta(Ro) \tag{9}$$

where $\langle\delta\theta_s\rangle$ represents an overall scaling of the SST anomalies:

$$\langle\delta\theta_s\rangle = u_m N^{3/2}/\left(g\alpha f^{1/2}\right) \tag{10}$$

In Figure 12, observed SST anomalies, $\delta\theta_s$, scaled by $\langle\delta\theta_s\rangle$ are compared to TC Rossby numbers. As obtained, the suggested scaling seems to well apply. Consistent with results numerously reported in literature, the higher the wind speed and the shallower the thermocline, larger shall be the SST anomalies. As well, the slower and larger the TC, more pronounced will also be the SST anomalies. While satisfactorily, clear scatter is still noticeable. It suggests that the overall $\langle\delta\theta_s\rangle$ is additionally impacted by other factors, in particular (as mentioned above) by the TC-induced upwelling impact.

Shown in Figure 13, SST wake offset, δx, and width, l, scaled by the radius of maximum wind speed are presented as a function of TC Rossby numbers. Again, conforming to previously reported observations (e.g.,

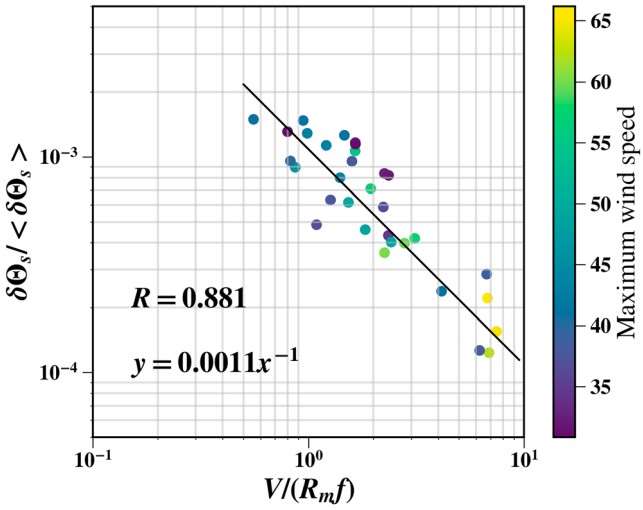

Figure 12. Observed sea surface temperature anomalies scaled by $\langle\delta\theta_s\rangle = u_m N^{3/2}/(g\alpha f^{1/2})$ versus tropical cyclone-Rossby number $Ro = V/(fR_m)$. Color indicates maximum wind speed. Solid line is the fit $\delta\theta_s/\langle\delta\theta_s\rangle = 1.1 \times 10^{-3} Ro^{-1}$.

D'Asaro et al., 2014), SST offsets (to the right from TC track) demonstrates a clear trend, increasing with increasing translation velocity.

3.2. SSH Anomalies

For the ocean surface height anomalies, δh_s, two contributions can be triggered: barotropic, δh_s^{bt} and baroclinic, δh_s^{bc}, as $\delta h_s = \delta h_s^{bt} + \delta h_s^{bc}$. For deep ocean conditions (depth about 5,000–7,000 m), δh_s^{bt} can be postulated much smaller than δh_s^{bc} (Geisler, 1970; Ginis & Sutyrin, 1995), and the barotropic contribution is further ignored in our analysis.

Invoking the pressure continuity condition at the surface, the following relationship is suggested between the surface vertical velocity, w_s, and the vertical velocity gradient, w_z', beneath the surface:

$$w_s = (C^2/g) w_z'|_{z=0} \tag{11}$$

where C is the phase velocity of long internal waves (see, e.g., equation (3.9) from Kudryavtsev et al., 2019). For a two-layer approximation (Geisler, 1970), with a very shallow upper layer, and constant densities in each layer, relation (11) can be simply estimated, using $C^2 = g(\Delta\rho/\rho) D$ and $w_z'|_{z=0} \simeq w_D/D$ as follows: $w_s = (\Delta\rho/\rho) w_D$, where $\Delta\rho/\rho$ is the density difference between layers scaled by the mean density value and w_D the vertical velocity of the pycnocline. Accordingly, compared to the pycnocline displacement, the surface displacement is attenuated by a factor $\Delta\rho/\rho$. As already discussed (see equation (5)), under a three-layer approximation, with constant density gradient in each layer, the vertical velocity in the upper seasonal thermocline layer becomes $w(z) \propto \sin(Nz/C)$, and equation (11) gives:

$$\delta h_s^{bc} \approx (NC/g)\delta D \tag{12}$$

where δD is the displacement of the base of the main pycnocline. As an estimate of this displacement, we follow Geisler (1970). For a two-layer ocean response to moving hurricanes, the amplitude, δD, (Geisler, 1970; equation(37)) becomes:

$$\delta D \propto \tau_s R_m/(CV) \tag{13}$$

where τ_s is the surface stress scaled by water density: $\tau_s = (\rho_a/\rho_w) C_d u_m^2$, C_d the surface drag coefficient. Accordingly, equation (12) becomes

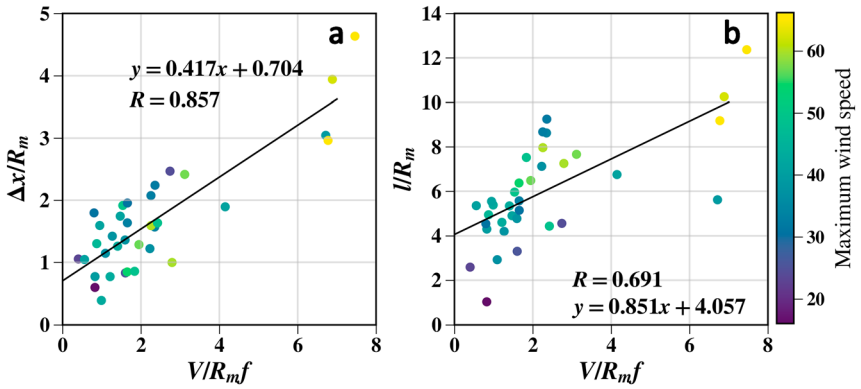

Figure 13. (a) Offset of sea surface temperature anomaly from tropical cycloneTC's track and (b) width of SST anomaly scaled by radius of maximum wind speed versus dimensionless translation velocity $Ro = V/(fR_m)$ (the tropical cyclone-Rossby number). Color indicates wind speed. Solid lines are fits to the data by least squares method.

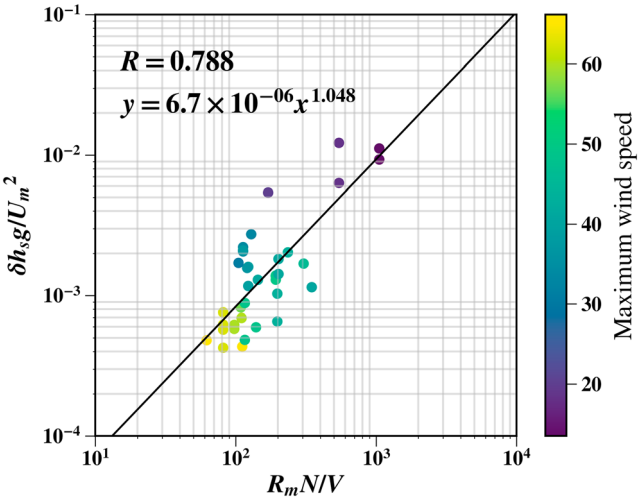

Figure 14. Dimensionless sea surface temperature anomalies, $\delta h_s^{bc} g/u_m^2$, versus parameter $R_m N/V$ (symbols). Solid line is the fit to the data using least squares method. Color indicates tropical cyclone maximal wind speed.

$$\delta h_s^{bc} \propto (\tau_s/g) R_m N_1/V \tag{14}$$

Assuming to first-order $\tau_s \propto u_m^2$, SSH anomalies shall scale as

$$\delta h_s^{bc} g/u_m^2 \propto R_m N/V \tag{15}$$

Dimensionless SSH anomalies as a function of parameter $R_m N/V$ are shown in Figure 14. In spite of a rather large scatter, essentially caused by residual SSH anomalies left by mesoscale activities and other possible preceding TCs, previously traveling in the same area, the data demonstrate a clear trend. A fit to correlate dimensionless SSH anomalies versus parameter $R_m N/V$, gives

$$\delta h_s^{bc} g/u_m^2 = 6.9 \times 10^{-6} (R_m N/V)^{1.04} \tag{16}$$

The fit exponent is close to 1, and the proportionality constant scales very well with a surface drag coefficient of order $C_d \propto 10^{-3}$ multiplied by $\rho_a/\rho_w \propto 10^{-3}$. This is further discussed in the next section.

4. Hurricane-Force Wind Forcing

Proper definition of the drag coefficient at high wind speed condition, above 30 m/s, is still a fundamental issue. As generally recognized, the relation for C_d valid for moderate winds must not be extrapolated to hurricane-force wind conditions. Scanty amount of observations indeed demonstrates that C_d levels off and/or falls at wind speeds above 30 m/s (e.g., Powell et al., 2003).

From the present analysis, equation (14) may well provide unique opportunities to assess drag coefficients from observed TC-induced SSH anomalies, δh_s^{bc}. To further dwell on this anticipated property, it is thus tempting to infer a drag coefficient dependency as function of the TC maximum winds, as

$$C_d \propto (\rho_w/\rho_a)(V/NR_m)\left(g h_s^{bc}/u_m^2\right) \tag{17}$$

Adjusted with a proportionality constant equal to 1/6, the predicted drag coefficients are reported in Figure 15. As proposed, this analysis bears strong resemblance with the bottom-up approach applied by Jarosz et al. (2007). These authors infer estimates of drag coefficients using ocean current profile measurements. Though the collected SSH anomalies are rather scattered, due to presence of residual SSH anomalies associated to mesoscale eddy activities and/or left by other previous TCs traveling in the same area before, the "su"ggested direct dependency (17) remarkably recovers an apparent drag reduction for wind speed higher than 35 m/s. This is in line with estimates reported by Powell et al. (2003) and Jarosz et al. (2007). Estimates also favorably compare with a top-down approach using observations of the height of the planetary boundary layer (Powell et al., 2003, Figure 2; Kudryavtsev, 2006, Figure 9).

Moreover, calculations of the surface stress, $\tau_s = C_d u^2$, shown in Figure 15b, reveal remarkable feature—the surface stress has a clear trend to level off at hurricane-force wind conditions. Model simulations by Kudryavtsev (2006) and Kudryavtsev and Makin (2011) provide some theoretical grounds to interpret this behavior. From the present analysis, the surface stress can be parameterized as

$$\tau_s = \left(\tau_{s0}^{-m} + \tau_{st}^{-m}\right)^{-1/m} \tag{18}$$

where τ_{s0} is a reference stress calculated with the drag coefficient corresponding to the Charnock roughness length $z_0 = 0.012 \times u_*^2/g$, and τ_{st} is a threshold value of the stress, m is a tuning exponent. Surface stress parameterization in equation (18) and corresponding drag coefficient, $C_d = \tau_s/u_m^2$ calculated for $m = 2$ and $\tau_{st} = 3$ m/s are reported in Figure 15; it fits the "cloud" of data and reproduce previously reported trends in the surface drag and the wind stress data.

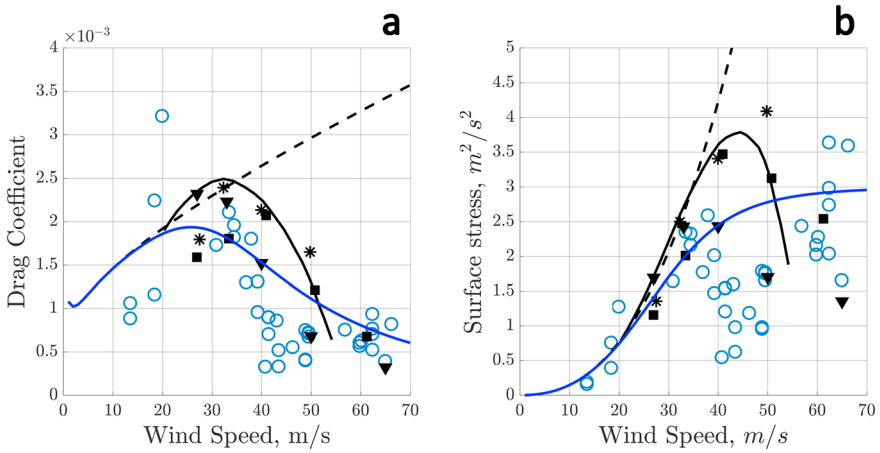

Figure 15. (a) Drag coefficient versus wind speed at 10-m height. Dashed line is C_d calculated for the roughness scale predicted by the Charnock relation: $z_0 = 0.12 \times u_*^2/g$; black squares are data by Powell (2006), compiled from his Figure 7, layer 20–160 m; stars are data by Powell et al. (2003) compiled from their Figure 3, layer 20–150 m; black solid line, fitted quadratic curve to the empirical data by Jarosz et al. (2007), their Figure 3; triangles are estimates by Kudryavtsev (2006); open circles show C_d derived from the altimeter SSH anomalies. (b) Corresponding surface stress versus wind speed calculated using C_d shown in Figure 12a.

5. Coupling Between SST and SSH Anomalies: Upwelling Mechanism Influence

As further interpreted, SSH anomalies provide direct estimates of the pycnocline upwelling associated to the passage of a TC. It can then be used to evaluate the upwelling impact, that is, the upwelling amplification, on the SST wake, equation (8). Using equation (12), this amplification factor can be expressed in terms of the SSH anomalies as

$$[1 + (N/C)\delta D] = 1 + g\delta h_s/C^2 \tag{19}$$

For the considered cases, SSH anomalies range from 0.1 to 0.5 m, and the IW phase velocities from 3 to 4 m/s, leading the amplification factor $(1+g\delta h_s/C^2)$ to vary between 1.1 and 1.5. The influence of the upwelling mechanism to control the strength of the SST wake is thus rather moderate. Nevertheless, the initial parameterization can now be extended, to explicitly introduce this upwelling factor as

$$\delta\theta_s/\langle\delta\theta_s\rangle = c_h\left[1 + c_u\frac{u_m^2}{C^2}\frac{N}{f}Ro^{-1}\right]Ro^{-1} \tag{20}$$

with, $\langle\delta\theta_s\rangle = u_m N^{3/2}/(g\alpha f^{1/2})$ representing an overall scaling of the SST anomalies, and c_h and c_u the empirical constants: $c_h = 0.8 \times 10^{-3}$ $c_u = 6.9 \times 10^{-6}$.

Observed versus predicted SST by equation (20) anomalies are reported in Figure 16. An overall agreement is clearly achieved, suggesting that equation (20) correctly includes fundamental mechanisms governing the expected strength of the SST wake. Deviations are likely caused by numerous other factors, that is, the precise TC shape, estimated radius of maximum winds and associated wind stress spatial distribution, departure of the vertical gradient from a constant value, etc. Peculiar upper ocean salinity distribution can also contribute to build potential energy barrier to mixing, thus reducing the cooling magnitude (Balaguru et al., 2012). Precise prediction of SST anomalies should thus certainly be performed using a more elaborated approach. Yet, to first order, accounting for all mentioned factors may not seem fully necessary, as essential constraining parameters are included within the proposed parameterization.

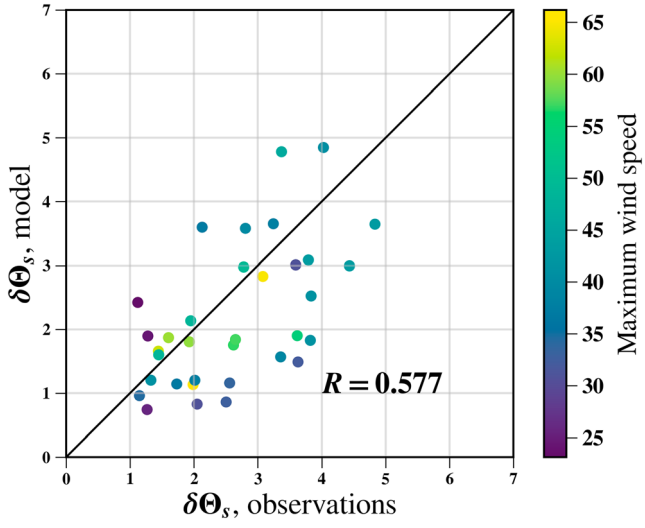

Figure 16. Scatter plot demonstrating relation of observed SST anomalies versus anomalies predicted by (20).

6. Summary

In the present paper, a consistent-parameterization framework has thus been developed to motivate a more systematic combination of SST and SSH satellite observations to analyze the ocean responses to TCs. This framework is demonstrated using 20-day satellite observations intercepting three major TC events, namely Jimena, Ignacio, and Kilo, developing and traveling over the central and eastern parts of the Pacific Ocean. As gathered, multisensor observations provide a comprehensive data set on local changes of SST (derived from passive microwave measurements) and SSH (altimeter measurements) along the TCs paths, sampling different stages of intensification, wind speeds, radii, Coriolis parameter, translation velocities, and ocean interior stratification conditions.

To first order, measured SST and SSH anomalies do not exhibit clear dependences on any "individual" TC characteristic (e.g., maximal wind speed, size, translation velocity), or environment interior condition, for example, stratification. Yet, as suggested, scaled SST and SSH anomalies can still be robustly predicted and combined.

As derived, a semiempirical relation to interpret SST anomalies can essentially build on the heat and momentum conservations laws for the upper wind driven mixed layer (ML). Considering that the bulk Richardson number of the ML deepening (combining drift current, temperature change over the ML base, and ML depth) keeps a constant (critical) value, the following relationship to explain SST anomalies writes:

$$\delta\theta_s/\langle\delta\theta_s\rangle = \varphi_\theta(V/R_m f)$$

where $\langle\delta\theta_s\rangle = u_m N^{3/2}/(g\alpha f^{1/2})$ is a scale of the SST anomalies, and φ_θ, a function of the dimensionless TC translation velocity, $V/R_m f$, found empirically as $\varphi_\theta = 1.1\times10^{-3}(V/R_m f)^{-1}$. The offset of the SST anomalies from the TC track is then mostly governed by the TC translation velocity: offsets are larger for faster TCs.

As collected, TC passages have further been found to strongly imprint the ocean surface height. For the considered TC cases, expected amplitudes of the barotropic responses to the TC transient forcing were expected to be small, limited to about 1 to 5 cm. This is much smaller than the reported SSH anomalies. Therefore, for these cases, SSH anomalies must essentially be governed by the ocean baroclinic response. Following Geisler (1970), scaling arguments to estimate the thermocline displacement induced by a moving TC, lead to the following relationship of SSH anomalies with TC and ocean interior parameters:

$$gh_s^{bc}/u_m^2 \propto R_m N_1/U$$

As demonstrated, this relationship may well provide unique opportunities to document the TC wind forcing and to assess drag coefficient from observed TC-induced SSH anomalies. From the collected SSH anomalies, a drag reduction is remarkably recovered for wind speed higher than 35 m/s, in line with estimates reported by Powell et al. (2003), Powell (2006) and Jarosz et al. (2007).

As interpreted, SSH anomalies thus provide direct estimates to evaluate the upwelling impact, that is, the upwelling amplification, on the SST wake. For the cases studied, the influence of the upwelling mechanism has been found to be rather moderate, of order 10–40%.

Building on the actual satellite altimeter constellation (presently up to six satellites are available), the proposed interpretation framework can thus guide the combined use of SST and SSH amplitude changes measured in the wakes of TCs. It can help to analyze the ocean response to TCs, and to first-order inform about the resulting strength of hurricane-induced mixing and upwelling. As mentioned above, the bottom-up approach can also guide future investigations to help document the resulting wind forcing and practical drag coefficient under extreme TC-conditions. In that context, it can also be anticipated that next NASA's Surface Water and Ocean Topography (Fu et al., 2012), with unprecedented 2-D altimeter mapping capabilities, certainly promises to greatly improve the analysis of TC-induced SSH wake: improved knowledge of the air-sea exchanges under TCs might thus be an unexpected outcome of this mission.

The proposed simplified framework is further extended in a 2019. It provides a more complete analytical description of ocean response to moving TC, especially detailing the wind-driven current field, ML

cooling and its evolution, and associated space–time variability of the pycnocline caused by TC-induced baroclinic motions.

Acknowledgments
The core support for this work was provided by the Russian Science Foundation through the project 17-77-30019 at Russian State Hydrometeorological University. The support from the Ministry of Science and Education (Goszadanie 5.2928.2017/PP) is also acknowledged. This study was also conducted within the Ocean Surface Topography Science Team (OSTST) activities. OSTST is led by CNES and NASA, and a grant was awarded by the TOSCA board to the SILLAGE project in the framework of the CNES/EUMETSAT Research Announcement CNES-DSP/OT 12-2118. The data used in this paper are available at http://data.remss.com/sst/daily_v04.0/mw/2015/, http://www.nodc.noaa.gov/, https://earth.esa.int/; http://www.aviso.altimetry.fr/, http://ftp.nhc.noaa.gov/atcf/, and https://www.nodc.noaa.gov/OC5/woa13/.

References

Babin, S. M., Carton, J. A., Dickey, T. D., & Wiggert, J. D. (2004). Satellite evidence of hurricane-induced phytoplankton blooms in an oceanic desert. *Journal of Geophysical Research*, *109*, C03043. https://doi.org/10.1029/2003JC001938

Balaguru, K., Chang, P., Saravanan, R., Leung, L. R., Xu, Z., Li, M., & Hsieh, J. S. (2012). Ocean barrier layers' effect on tropical cyclone intensification. *Proceedings of the National Academy of Sciences*, *109*(36), 14,343–14,347. https://doi.org/10.1073/pnas.1201364109

Cornillon, P., Stramma, L., & Price, J. F. (1987). Satellite measurements of sea surface cooling during hurricane Gloria. *Nature*, *326*(6111), 373–375. https://doi.org/10.1038/326373a0

D'Asaro, E. A., Black, P. G., Centurioni, L. R., Chang, Y.-T., Chen, S. S., Foster, R. C., et al. (2014). Impact of typhoons on the ocean in the Pacific. *Bulletin of the American Meteorological Society*, *95*(9), 1405–1418. https://doi.org/10.1175/BAMS-D-12-00104.1

Emanuel, K. A. (2005). Increasing destructiveness of tropical cyclones over the past 30 years. *Nature*, *436*(7051), 686–688. https://doi.org/10.1038/nature03906

Fu, L. L., Alsdorf, D., Morrow, R., Rodriguez, E., & Mognard, N. (2012). *SWOT: The surface water and ocean topography mission: Wide-swath altimetric elevation on Earth*. Pasadena, CA: Jet Propulsion Laboratory, National Aeronautics and Space Administration.

Geisler, J. E. (1970). Linear theory of the response of a two layer ocean to a moving hurricane. *Geophysical and Astrophysical Fluid Dynamics*, *1*(1-2), 249–272. https://doi.org/10.1080/03091927009365774

Gill, A. E. (1984). On the behavior of internal waves in the wakes of storms. *Journal of Physical Oceanography*, *14*(7), 1129–1151. https://doi.org/10.1175/1520-0485(1984)014<1129:OTBOIW>2.0.CO;2

Ginis, I. (2002). Tropical cyclone-ocean interactions. *Advances in Fluid Mechanics*, *33*, 83–114.

Ginis, I., & Sutyrin, G. (1995). Hurricane-generated depth-averaged currents and sea surface elevation. *Journal of Physical Oceanography*, *25*(6), 1218–1242. https://doi.org/10.1175/1520-0485(1995)025<1218:HGDACA>2.0.CO;2

Grodsky, S. A., Reu, N., Reverdin, G., Carton, J. A., Chapron, B., Quilfen, Y., et al. (2012). Haline hurricane wake in the Amazon/Orinoco plume: AQUARIUS/SACD and SMOS observations. *Geophysical Research Letters*, *39*, L20603. https://doi.org/10.1029/2012GL053335

Huang, S. M., & Oey, L. Y. (2015). Right-side cooling and phytoplankton bloom in the wake of a tropical cyclone. *Journal of Geophysical Research: Oceans*, *120*, 5735–5748. https://doi.org/10.1002/2015JC010896

Hwang, P. A., & Fan, Y. (2017). Effective fetch and duration of tropical cyclone wind fields estimated from simultaneous wind and wave measurements: Surface wave and air-sea exchange computation. *Journal of Physical Oceanography*, *47*(2), 447–470. https://doi.org/10.1175/JPO-D-16-0180.1

Jansen, M. F., Ferrari, R., & Mooring, T. A. (2010). Seasonal versus permanent thermocline warming by tropical cyclones. *Geophysical Research Letters*, *37*, L03602. https://doi.org/10.1029/2009GL041808

Jarosz, E., Mitchell, D. A., Wang, D. W., & Teague, W. J. (2007). Bottom-up determination of air-sea momentum exchange under a major tropical cyclone. *Science*, *315*(5819), 1707–1709. https://doi.org/10.1126/science.1136466

Kolodziejczyk, N., Prigent-Mazella, A., & Gaillard, F. (2017). *ISAS-15 temperature and salinity gridded fields*. SEANOE. http://doi.org/10.17882/52367

Kudryavtsev, V., Golubkin, P., & Chapron, B. (2015). A simplified wave enhancement criterion for moving extreme events. *Journal of Geophysical Research: Oceans*, *120*, 7538–7558. https://doi.org/10.1002/2015JC011284

Kudryavtsev, V., & Makin, V. (2011). Impact of ocean spray on the dynamics of the marine atmospheric boundary layer. *Boundary-Layer Meteorology*, *140*(3), 383–410. https://doi.org/10.1007/s10546-011-9624-2

Kudryavtsev, V., Monzikova, A., Combot, C., Chapron, B., & Reul, N. (2019). A simplified model for thebaroclinic and barotropic ocean-response to moving tropical cyclones: 2.Model and simulations. *Journal ofGeophysical Research: Oceans*, *124*. https://doi.org/10.1029/2018JC014747

Kudryavtsev, V. N. (2006). On the effect of sea drops on the atmospheric boundary layer. *Journal of Geophysical Research*, *111*, C07020. https://doi.org/10.1029/2005JC002970

Lin, I. I., Chen, C. H., Pun, I. F., Liu, W. T., & Wu, C. C. (2009). Warm ocean anomaly, air sea fluxes, and the rapid intensification of tropical cyclone Nargis (2008). *Geophysical Research Letters*, *36*, L03817. https://doi.org/10.1029/2008GL035815

Lin, S., Zhang, S.-P., Shang, W.-Z., & Hong, H.-S. (2017). Ocean response to typhoons in the western North Pacific: Composite results from Argo data. *Deep–Sea Research Part I 123* 62–74

Longuet-Higgins, M. S. (1965). The response of a stratified ocean to stationary or moving wind-systems. *Deep Sea Research and Oceanographic Abstracts*, *12*(6), 923–973. https://doi.org/10.1016/0011-7471(65)90814-4

Mei, W., Pasquero, C., & Primeau, F. (2012). The effect of translation speed upon the intensity of tropical cyclones over the tropical ocean. *Geophysical Research Letters*, *39*, L07801. https://doi.org/10.1029/2011GL050765

Meroni, A. N., Miller, M. D., Tziperman, E., & Pasquero, C. (2017). Nonlinear energy transfer among ocean internal waves in the wake of a moving cyclone. *Journal of Physical Oceanography*, *47*(8), 1961–1980. https://doi.org/10.1175/JPO-D-16-0232.1

Powell, M. D. (2006). Drag coefficient distribution and wind speed dependence in tropical cyclones. Final report to the National Oceanic and Atmospheric Administration, Joint Hurricane Testbed Program, *Miami*, 26 pp.

Powell, M. D., Vickery, P. J., & Reinhold, T. A. (2003). Reduced drag coefficient for high wind speeds in tropical cyclones. *Nature*, *422*(6929), 279–283. https://doi.org/10.1038/nature01481

Price, J. F. (1981). Upper ocean response to a hurricane. *Journal of Physical Oceanography*, *11*(2), 153–175. https://doi.org/10.1175/1520-0485(1981)011<0153:UORTAH>2.0.CO;2

Price, J. F. (1983). Internal wave wake of a moving storm. Part I. Scales, energy budget and observations. *Journal of Physical Oceanography*, *13*(6), 949–965. https://doi.org/10.1175/1520-0485(1983)013<0949:IWWOAM>2.0.CO;2

Price, J. F., Weller, R. A., & Pinkel, R. (1986). Diurnal cycling: Observations and models of the upper ocean response to diurnal heating, cooling, and wind mixing. *Journal of Geophysical Research*, *91*(C7), 8411–8427. https://doi.org/10.1029/JC091iC07p08411

Pudov, V., & Petrichenko, S. (2000). Trail of a typhoon in the salinity field of the ocean upper layer. *Atmospheric and Oceanic Physics*, *36*, 700–706.

Reul, N., Chapron, B., Lee, T., Donlon, C., Boutin, J., & Alory, G. (2014). Sea surface salinity structure of the meandering Gulf Stream revealed by SMOS sensor. *Geophysical Research Letters*, *41*, 3141–3148. https://doi.org/10.1002/2014GL059215

Reul, N., Chapron, B., Zabolotskikh, E., Donlon, C., Mouche, A., Tenerelli, J., et al. (2017). A new generation of tropical cyclone size measurements from space. *Bulletin of the American Meteorological Society*, *98*(11), 2367–2385. https://doi.org/10.1175/BAMS-D-15-00291.1

Shay, L. K. (2010). Air-sea interactions intropical cyclones. In J. C. L. Chan & J. Kepert (Eds.). *Global Perspectives of Tropical Cyclones*, *World Scientific PublishingCompany: Earth System Science Publication Series* (Chap. 3, 2nd ed.), London, UK, 93–131. https://doi.org/10.1142/9789814293488_0003

Skyllingstad, E. D., Smyth, W. D., & Crawford, G. B. (2000). Resonant wind-driven mixing in the ocean boundary layer. *Journal of Physical Oceanography*, *30*(8), 1866–1890. https://doi.org/10.1175/1520-0485(2000)030<1866:RWDMIT>2.0.CO;2

Vincent, E. M., Lengaigne, M., Madec, G., Vialard, J., Samson, G., Jourdain, N. C., et al. (2012). Processes setting the characteristics of sea surface cooling induced by tropical cyclones. *Journal of Geophysical Research*, *117*, C02020. https://doi.org/10.1029/2011JC007396

Vincent, E. M., Lengaigne, M., Vialard, J., Madec, G., Jourdain, N. C., & Masson, S. (2012). Assessing the oceanic control on the amplitude of sea surface cooling induced by tropical cyclones. *Journal of Geophysical Research*, *117*, C05023. https://doi.org/10.1029/2011JC007705

Walker, N. D., Leben, R. R., & Balasubramanian, S. (2005). Hurricane-forced upwelling and chlorophyll *a* enhancement within cold-core cyclones in the Gulf of Mexico. *Geophysical Research Letters*, *32*, L18610. https://doi.org/10.1029/2005GL023716

Wright, C. W., Walsh, E. J., Vandemark, D., Krabill, W. B., Garcia, A. W., Houston, S. H., et al. (2001). Hurricane directional wave spectrum spatial variation in the open ocean. *Journal of Physical Oceanography*, *31*(8), 2472–2488. https://doi.org/10.1175/1520-0485(2001)031<2472:HDWSSV>2.0.CO;2

Yablonsky, R. M., & Ginis, I. (2009). Limitation of one-dimensional ocean models for coupled hurricane–ocean model forecasts. *Monthly Weather Review*, *137*(12), 4410–4419. https://doi.org/10.1175/2009MWR2863.1